Physical Insight Into Frequency-Dependent Nonlinearities in AlGaN/GaN HEMTs

Sergio García-Sánchez, Ignacio Íñiguez-de-la-Torre, Gaudencio Paz-Martínez, Philippe Artillan, Tomás González, *Senior Member, IEEE*, and Javier Mateos, *Member, IEEE*

***Abstract*—We investigate the frequency-dependent nonlinearities of an AlGaN/GaN high electron mobility transistor (HEMT) involved in terahertz (THz) detection by means of two-dimensional Monte Carlo (MC) simulations. The analysis shows that, below 1 THz, the responsivity roll-off is mainly governed by the passive microwave behavior of the device rather than by any limitation of the intrinsic detection mechanism. At higher frequencies, an inverse extraction method able to provide the intrinsic nonlinearity coefficients of the device, reveals just a marginal broad enhancement around 1 THz followed by a steep roll-off.**

***Index Terms*—GaN high electron mobility transistors (HEMTs), Millimeter wave (mmWave) detection, Monte Carlo simulations, Zero-bias detector.**

I. Introduction

Terahertz (THz) radiation, located between microwaves and infrared on the electromagnetic spectrum, offers significant potential for various applications including imaging, spectroscopy, and high-speed communication [1], [2]. However, the accurate detection of THz power presents several challenges that researchers are actively addressing. In this regard, Field-Effect Transistors (FETs) are emerging as highly competitive devices for THz detection, offering several compelling advantages over the well-established Schottky diode technology [3]. While Schottky barrier diodes (SBDs) remain a mature technology with very good performance in terms of speed and low noise for certain THz applications [4], some of the advantages of the THz detection with FETs, apart from the possibility of a seamless integration with CMOS platforms, are related to the flexibility in the design (mainly associated to the impedance matching) provided by the presence of the gate terminal, allowing for a certain tunability of the detector input impedance. Also, they show superior noise performance, since the resistance of FETs can be very effectively reduced by means of using high mobility semiconductors and appropriately scaling their dimensions.

Since the concept of plasma-wave detectors (following the Dyakonov-Shur theory [5]) was coined, many efforts have been done to improve the detection performance, both in terms of responsivity and sensitivity, or Noise Equivalent power (NEP) at high frequencies, ideally reaching the sub-THz and THz range [1]. The Dyakonov-Shur theory describes how a two-dimensional electron fluid in a field-effect transistor (FET) can support plasma waves, which can be excited by incident THz radiation. These plasma oscillations at THz frequencies contribute to the device's ability to detect signals much above their amplification cutoff frequencies (f_t and f_{max}) [6]. Despite decades of research, there has been ongoing discussion regarding the precise detection mechanisms in FETs [7], indeed, it is not yet completely understood how the resistive-mixing mechanism (associated to the non-linear I-V curve of the devices), active at low frequencies, is substituted by other mechanisms such as thermoemission or plasma-wave related detection mechanisms, as the frequency is increased [8].

This work tries to shed light on this problem focusing on GaN HEMTs, but its conclusions may be generalized to other FET technologies (such as InP HEMTs or Si MOSFETs). By using a generalized model for RF power detection, we will present here the numerical framework based on microscopic Monte Carlo (MC) simulations for extracting the frequency-dependent nonlinearity parameters, which can be considered as the "detection sources" and be used to model the performance of FETs as AC power detectors up to THz frequencies. Such intrinsic MC simulations allow to remove the effects of the device parasitics (very significant at THz frequencies, which hinder the understanding of experimental results), and isolate the intrinsic mechanisms at the origin of RF power detection with FETs. We will demonstrate that the intrinsic nonlinearity of the device does not clearly show the expected plasma resonance at THz frequencies, but a marginal broad enhancement at around 1 THz (never higher than a 10% with respect to the low frequency value).

II. Simulator and device details

The device is modeled using a two-dimensional (2D) semiclassical ensemble MC solver, self-consistently coupled with the Poisson equation [9], [10] which includes all the microscopic mechanisms at the origin of THz detection, namely, current non-linearity, collective phenomena as plasma waves, electron heating and thermoemission, carrier inertia,

This work has been partially supported through grants PID2023-147555OB-I00 and PDC2023-145896-I00 funded by MCIN/AEI/10.13039/501100011033, the Junta de Castilla y León and FEDER through project SA136P23, and the Fundación General de la Universidad de Salamanca through project PC_TCUE25_004. This research has made use of the high performance computing resources of the Castilla y León Supercomputing Center (SCAYLE, www.scayle.es), financed by the European Regional Development Fund (ERDF). (*Corresponding author: Sergio García-Sánchez*)

S. García-Sánchez, I. Íñiguez-de-la-Torre, G. Paz-Martínez, T. González and J. Mateos are with with the Applied Physics Department, and USAL-NANOLAB, Universidad de Salamanca, 37008 Salamanca, Spain (e-mail: sergio_gs@usal.es, indy@usal.es, gaupaz@usal,es, tomasg@usal.es and javierm@usal.es). P. Artillán is with Univ. Grenoble Alpes, Univ. Savoie Mont Blanc, CNRS, Grenoble INP, CROMA, Grenoble, France. (e-mail: philippe.artillan@univ-smb.fr).

etc. Electron dynamics are computed in 1 fs steps, accounting for intervalley, acoustic and optical phonon, piezoelectric, and ionized impurity scattering. More details are provided in Ref. [10]. The AlGaN/GaN HEMT features a 150 nm gate length, with 300 nm and 750 nm source-to-gate and gate-to-drain spacings. The epitaxial stack includes a 0.5 nm GaN cap, 14 nm AlGaN barrier, 1 nm AlN interlayer, and 250 nm GaN channel, as shown in the sketch in the inset of Fig. 1. The intrinsic I_d-V_{ds} curves obtained directly from MC simulations are plotted in Fig. 1, while the inset shows the excellent agreement with the measurements made on a device with the same geometry [11] once the contact resistances and the Schottky barrier height are accounted for, using the same procedure as in Ref. [10]. We have to remark here that MC simulations of ohmic contacts involve the direct injection of electrons into the 2DEG channel, and also a shortened source-gate distance (0.3 μm instead of 1.6 μm), so that the value for the contact resistance is slightly higher than the experimental one.

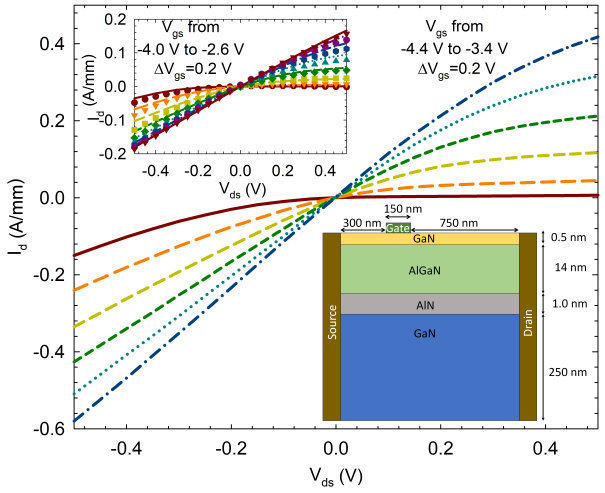

Fig. 1. Intrinsic I_d–V_{ds} output characteristics at low V_{ds}. The inset shows the good agreement with measurements in a similar device achieved by adding to the simulations the effect of the contact resistances (with a total value of 2.0 Ω·mm, in good agreement with the measured data) and the Schottky barrier height at the gate terminal (0.71 V). A sketch of the simulated device (not to scale) is also included.

III. AC Power Detection

A. RF Power Detection Simulations: Gate-port with RF Short-Circuit and Matched Load Connections

In order to correctly account for RF power reflection and transmission imposed by the device under test, their S-parameters are initially obtained by means of MC simulations by transformation of the Y-parameters computed by applying single-tone voltage excitations and recording the current response [12]. Afterwards, the detection operation under drain-injection conditions is simulated. First, the frequency-dependent current responsivity with the gate port terminated with a RF short circuit, $\beta_d^{MCsh}(f)$, is obtained from time-domain MC simulations by applying a sinusoidal signal with varying f to the drain terminal, v_{ds}^{sh}, while keeping the gate voltage constant at its dc value, V_{gs} (more details are given in Ref. [10]). Under these conditions the RF drain-gate coupling is canceled, thus simplifying the analytical interpretation of the result, as will be explained later. The simulated rectified drain current, $\Delta I_d(f)$, allows to calculate $\beta_d^{MCsh}=\frac{\Delta I_d}{P_S}$ where $P_S=\frac{v_S^2}{8Z_S}$ is the power injected by the RF power source (with amplitude v_S) and Z_S the source impedance.

As second step, the responsivity with RF matched gate port $\beta_d^{MCmg}(f)$ is obtained in a similar way, but in this case sinusoidal signals dependent on f (v_{ds}^{mg} and v_{gs}^{mg}) are applied to both drain and gate contacts computed using the previously extracted S-parameters of the device:

$$\begin{aligned} v_{ds}^{mg}(t) &= \Re\left[(1+S_{22})\, v_S\, e^{j2\pi ft}/2\right]; \\ v_{gs}^{mg}(t) &= V_{gs} + \Re\left[S_{12}\, v_S\, e^{j2\pi ft}/2\right]; \\ v_{ds}^{sh}(t) &= \Re\left[\left(1+\Gamma_{\text{in}}^{sh}(f)\right) v_S\, e^{j2\pi ft}/2\right]; \\ v_{gs}^{sh}(t) &= V_{gs}, \end{aligned} \tag{1}$$

where $\Gamma_{\text{in}}^{sh}(f)$ is the input reflection coefficient at the drain terminal, which, under short-circuited-gate-conditions, takes a value of $\Gamma_{\text{in}}^{sh}(f)=S_{22}(f)-\frac{S_{21}(f)S_{12}(f)}{1+S_{11}(f)}$.

B. Analytical Formalism Based on the Non-linearity of the I_d–V_{ds} Curves and S-Parameters

If one assumes that the frequency of the AC excitation is low enough, *i.e.* the resistive-mixing mechanism is at the origin of the RF power detection and its frequency dependence is just provided by the input RF power reflected and transmitted by the transistor (and thus related to its S-parameters), simple closed-form (CF) expressions (extracted in Ref. [13], [14] by these authors) can be used to obtain the frequency-dependent RF power responsivity of any kind of FET. Under these conditions, the non-linearity of the I_d–V_{ds} curves, shown in Fig. 1, represented by the frequency-independent g_{ij} coefficients (defined as the second order derivatives of I_d vs. V_{ds} and V_{gs}, $g_{ij}=\frac{\partial^{(i+j)}I_d}{\partial^i V_{gs}\partial^j V_{ds}}$), is the mechanism at the origin of the RF power detection.

In contrast, when increasing the excitation frequency, carrier inertia, plasma and thermoemission effects start to be significant and, as a consequence, the assumption of constant g_{ij} values does not hold anymore. As a first approximation, one can obtain their frequency dependence from MC simulations via the Y-parameters of the device. First, the drain conductance $g_{01}(f)$ is obtained as the real part of $Y_{22}(f)$ (computed by applying a small-signal excitation at the drain [12]) and the coefficients $g_{11}(f)$ and $g_{02}(f)$ are then derived using finite-difference approximations based on incremental variations of the gate and drain dc bias, respectively. The results obtained with this calculation, see Fig. 2(a), as expected, show a low-frequency plateau until about 100 GHz, where a frequency dependence starts to be evident, displaying a plasma-related enhancement at about 1 THz. Moreover, their values approximately satisfy the condition $g_{11} \approx -g_{02}$, as expected, since the variations of the drain conductance take opposite sign when varying V_d and V_g, as they are controlled by the value of $\Delta V_{gs} = \Delta V_{gd}$ (the transistor is at zero-drain bias).

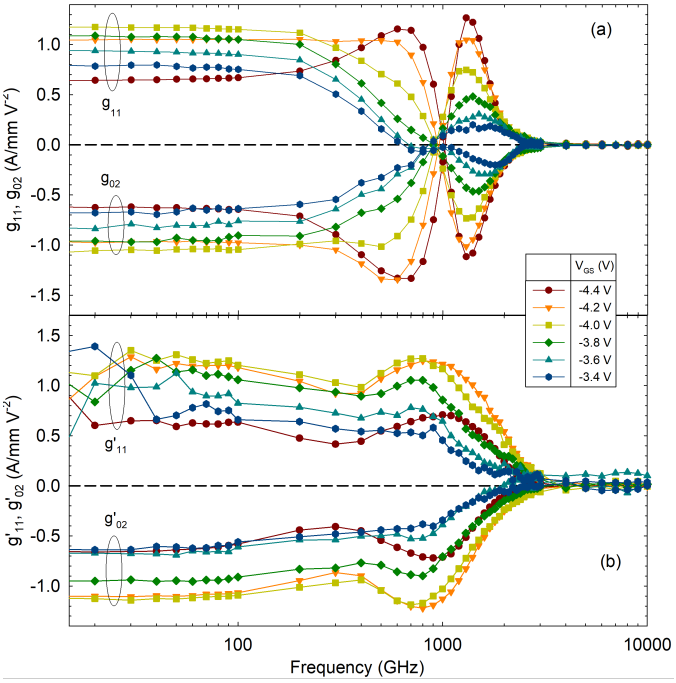

Fig. 2. Comparison between (a) derivative-based (g_{ij}) and (b) inverse-extracted (g'_{ij}) nonlinear coefficients for different V_{gs}.

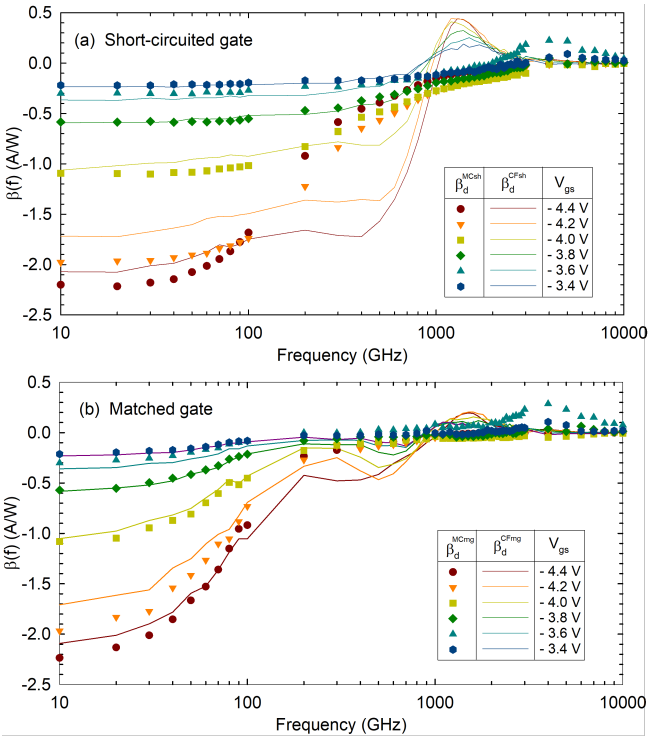

Fig. 3. Comparison of the responsivities obtained with direct MC computation and by reconstruction from CF expressions under (a) short-circuited gate configuration: β_d^{MCsh} (symbols) and β_d^{CFsh} (lines) and (b) matched gate configuration: β_d^{MCmg} (symbols) and β_d^{CFmg} (lines). Results are shown for different gate biases V_{gs}.

However, this initial calculation of the $g_{ij}(f)$ coefficients is not correct, as it does not take into account the frequency dependency of the non-linearity, since it assumes that the variations of $Y_{22}(f)$ when applying time-varying V_{ds} and V_{gs} voltages take place instantaneously. As such, only the frequency dependence of the linear response of the devices is accounted for. This fact is clearly demonstrated by the results shown in Fig. 3, where one can observe that the values of the responsivities (both in short-circuit and matched gate configurations) obtained with the (i) direct MC computation and by (ii) reconstructing them from the CF expressions do not align at frequencies above 100 GHz, just when the $g_{ij}(f)$ coefficients start to be frequency dependent.

For this reason, we propose an alternative strategy based on the inverse extraction of the effective non-linearity coefficients $g'_{ij}(f)$. They are computed from the simulations of the responsivities $\beta_d^{MCsh}(f)$ and $\beta_d^{MCmg}(f)$ by knowing their relationship with $g'_{ij}(f)$ given by the analytical CF expressions of $\beta_d^{CF'sh}(f)$ and $\beta_d^{CF'mg}(f)$, the latter derived in Ref. [10], while the former can be straightforwardly obtained in a similar way. The extraction of the frequency-dependent coefficient $g'_{02}(f)$ is performed by isolating the direct-drain contribution to the responsivity, $\beta_d^{MCsh}(f)$, obtained from MC simulations under short-circuited gate conditions. This corresponds to the $\beta_{DD}(f)$ term in the CF analytical expression of the responsivity (see Refs. [13], [14]), which can be rewritten as:

$$\beta_d^{MCsh}(f) = \beta_d^{CF'sh}(f) = \frac{R_0}{2}\left(g'_{02}(f)|1+\Gamma_{\text{in}}^{sh}(f)|^2\right). \quad (2)$$

Once $g'_{02}(f)$ has been determined from the short-circuited gate configuration, we extract $g'_{11}(f)$ by isolating the drain-gate coupling contribution in the CF expression for $\beta_d^{CF'mg}(f)$, which under these conditions is given by:

$$\beta_d^{MCmg}(f) = \beta_d^{CF'mg}(f) = \frac{R_0}{2}\Big[g'_{02}(f)\,|1+\Gamma_{\text{in}}^{mg}(f)|^2 + 2g'_{11}(f)\,\text{Real}\big\{S_{12}^*(f)[1+\Gamma_{\text{in}}^{mg}(f)]\big\}\Big] \quad (3)$$

where Γ_{in}^{mg}=S_{22} in matched-gate conditions, so that solving for $g'_{11}(f)$ its value can be obtained.

As can be seen in Fig. 2, apart from their low frequency values, the results obtained for $g_{ij}(f)$ and $g'_{ij}(f)$ are quite different. The resonant behavior of $g_{ij}(f)$ with a crossing point around 1 THz, turns into a smoother behavior with a broad peak around that same frequency. Instead of the expected enhancement of the THz detection predicted by the plasma-wave theory, practically only a frequency roll-off (with a -3 dB cut-off frequency around 2 THz, which decreases with increasing V_{gs}) of the non-linearity mechanism is observed, see Fig. 2(b). This means that the lower frequency cut-off of the responsivity observed in Fig. 3 is mainly due to the passive filtering of the response due to the presence of the device capacitances, and not to a frequency dependence of its intrinsic nonlinearity. It is also remarkable that the broad peak of the responsivity observed at around 4 THz for V_{gs}=-3.6 V, Fig. 3, translates into a practically flat value of $g'_{ij}(f)$ above 3 THz, Fig. 2(b), small with respect to its low frequency value (and with opposite sign). This high frequency detection resonance, according to the CF expressions, is due to the frequency

dependence of S parameters (see Ref [10]), and may be linked to plasma resonances coupled with thermoemission process at the source-gate region, as explained in Refs. [8], [15].

IV. CONCLUSION

By means of MC simulations, we have extracted the values of the frequency-dependent nonlinearity coefficients at the origin of the detection provided by GaN HEMTs. Using this result, we have demonstrated that the frequency roll-off of the responsivity at frequencies below 1 THz is not caused by the intrinsic physical phenomena at the origin of the detection, but by the passive microwave behavior of the transistor. However, the negative influence of the gate capacitances of the transistors when used as amplifiers (sharply degrading their high-frequency performance) is not a problem for their operation as detectors. On the contrary, they are even beneficial, as short-circuiting gate and drain or source terminals (often realized by a large capacitor in practical implementations of FET-based THz detectors [8], [16]) can improve the detected drain current output. Also, the transconductance, g_m, plays a key role for improving the amplifier gain, but has no influence in the detection (g_m is null at zero drain bias), Therefore, low mobility materials such as GaN or Si can provide optimum detection performances, and there is no need for ultra-short gate length designs. Indeed, different design rules must be applied for the optimization of FETs as detectors, which could be obtained by using the CF formalism and the values of the $g'_{ij}(f)$ coefficients obtained here , and combined with an equivalent circuit modelling approach for the transistors (as done in Ref. [17] taking as a base the experimental results).

REFERENCES

[1] X. Li, J. Li, Y. Li, A. Ozcan, and M. Jarrahi, "High-throughput terahertz imaging: progress and challenges," *Light: Science & Applications*, vol. 12, no. 1, p. 233, 2023.

[2] X. Fu, Y. Liu, Q. Chen, Y. Fu, and T. J. Cui, "Applications of terahertz spectroscopy in the detection and recognition of substances," *Frontiers in Physics*, vol. 10, p. 869537, 2022.

[3] E. Javadi, D. B. But, K. Ikamas, J. Zdanevičius, W. Knap, and A. Lisauskas, "Sensitivity of field-effect transistor-based terahertz detectors," *Sensors*, vol. 21, no. 9, 2021.

[4] J. Martinez-Gil, I. Belio-Apaolaza, J. Tebart, J. L. Fernández Estévez, D. Moro-Melgar, C. C. Renaud, A. Stöhr, and O. Cojocari, "Performance Evaluation of GaAs and InGaAs Schottky Mixers at 0.3 THz: A Comparative Analysis Between Optical and Electrical Pumping in THz Wireless Communication Systems," *Electronics*, vol. 14, no. 10, p. 1957, 2025.

[5] M. I. Dyakonov and M. S. Shur, "Plasma wave electronics: novel terahertz devices using two dimensional electron fluid," *IEEE Transactions on Electron Devices*, vol. 43, no. 10, pp. 1640–1645, 1996.

[6] V. Ryzhii, C. Tang, T. Otsuji, M. Ryzhii, V. Mitin, and M. Shur, "Resonant plasmonic detection of terahertz radiation in field-effect transistors with the graphene channel and the black-As x P 1-x gate layer," *Scientific Reports*, vol. 13, no. 1, p. 9665, 2023.

[7] J. Marczewski, M. Zaborowski, D. Tomaszewski, P. Zagrajek, and N. Pałka, "Why FETs detect a THz signal at a frequency far beyond their amplifying capabilities," *Opto-Electronics Review*, vol. 32, no. 4, 2024.

[8] F. Ludwig, A. Generalov, J. Holstein, A. Murros, K. Viisanen, M. Prunnila, and H. G. Roskos, "Terahertz detection with graphene FETs: Photothermoelectric and resistive self-mixing contributions to the detector response," *ACS Applied Electronic Materials*, vol. 6, no. 4, pp. 2197–2212, 2024.

[9] J. Mateos, T. González, D. Pardo, V. Hoël, and A. Cappy, "Monte Carlo simulator for the design optimization of low-noise HEMTs," *IEEE Transactions on Electron Devices*, vol. 47, no. 10, pp. 1950–1956, 2000.

[10] S. García-Sánchez, I. Íñiguez-de-la Torre, G. Paz-Martínez, P. Artillan, T. González, and J. Mateos, "Analysis of the THz Responsivity of AlGaN/GaN HEMTs by Means of Monte Carlo Simulations," *IEEE Transactions on Electron Devices*, 2024.

[11] S. Rennesson, F. Lecourt, N. Defrance, M. Chmielowska, S. Chenot, M. Lesecq, V. Hoel, E. Okada, Y. Cordier, and J.-C. De Jaeger, "Optimization of $\mathrm{al_{0.29}ga_{0.71}n/gan}$ high electron mobility heterostructures for high-power/frequency performances," *IEEE Transactions on Electron Devices*, vol. 60, no. 10, pp. 3105–3111, 2013.

[12] A. Afzali-Kushaa and G. I. Haddad, "High frequency characteristics of MESFETs," *Solid-state electronics*, vol. 38, no. 2, pp. 401–406, 1995.

[13] G. Paz-Martínez, P. Artillan, J. Mateos, E. Rochefeuille, T. González, and I. Íñiguez-De-La-Torre, "A closed-form expression for the frequency-dependent microwave responsivity of transistors based on the I–V curve and s-parameters," *IEEE Transactions on Microwave Theory and Techniques*, vol. 72, no. 1, pp. 415–420, 2023.

[14] P. Artillan, I. Íñiguez-de-la Torre, G. Paz-Martínez, E. Rochefeuille, S. García-Sánchez, T. González, and J. Mateos, "Multiport square law detectors: Responsivity matrix model and direct determination of the optimum injection regime," *IEEE Trans. Microw. Theory Tech.*, vol. 72, no. 10, pp. 6044–6048, 2024.

[15] J. Mateos and T. Gonzalez, "Plasma enhanced terahertz rectification and noise in InGaAs HEMTs," *IEEE Transactions on Terahertz Science and Technology*, vol. 2, no. 5, pp. 562–569, 2012.

[16] M. Bauer, A. Rämer, S. A. Chevtchenko, K. Y. Osipov, D. Čibiraitė, S. Pralgauskaitė, K. Ikamas, A. Lisauskas, W. Heinrich, V. Krozer, and H. G. Roskos, "A high-sensitivity AlGaN/GaN HEMT terahertz detector with integrated broadband bow-tie antenna," *IEEE Transactions on Terahertz Science and Technology*, vol. 9, no. 4, pp. 430–444, 2019.

[17] G. Paz-Martínez, I. Íñiguez-de-la Torre, P. Artillan, E. Rochefeuille, S. García-Sánchez, T. González, and J. Mateos, "Small-signal equivalent circuit model as a tool for optimizing millimeter-wave detection with FETs," *IEEE Transactions on Electron Devices*, vol. 71, no. 9, pp. 5225–5232, 2024.